Growth and structure of small gold particles on rutile TiO_2(110)

Devina Pillay and Gyeong S. Hwang*
Department of Chemical Engineering and Institute of Theoretical Chemistry, The University of Texas at Austin, Austin, Texas 78712, USA

(Received 6 May 2005; revised manuscript received 15 July 2005; published 15 November 2005)

The growth and structure of small Au_n particles ($n=1$–4) on a rutile TiO_2(110) surface have been examined using gradient corrected density functional theory slab calculations. We present potential energy maps for single Au atoms on the stoichiometric and reduced surfaces. This comparison shows that the presence of oxygen vacancies on TiO_2(110) drastically alters the adsorption and surface diffusion of single Au atoms, and in turn the growth and structure of Au particles. On the reduced surface, the delocalization of electrons from oxygen vacancies provides a low-energy diffusion channel for Au adatoms along a Ti($5c$) row, while there is no preferential direction in Au diffusion on the stoichiometric surface. The small Au particles bind preferably to the vacancy site, with a sizable adsorption energy that oscillates with the number of constituent atoms by virtue of spin pairing. Based on the comparison of supported and gas-phase Au particles, we also discuss the effect of the particle-substrate interaction on the structure of small Au particles grown on TiO_2(110).

DOI: 10.1103/PhysRevB.72.205422 PACS number(s): 68.35.−p, 61.46.+w, 68.43.−h

I. INTRODUCTION

Gold nanoparticles dispersed on titania exhibit an extraordinarily high activity for various low-temperature oxidation processes,[1,2] while its bulk form has been known to be chemically inert. The catalytic activity of supported Au particles is very sensitive to their size,[3] and this activity is optimal when the particle diameter is in the range from 2 to 3 nm.[1] Thus, it is important to tune the structural properties of supported Au particles to achieve high catalytic activity.

Oxide-supported metal catalysts have widely been prepared by vapor deposition of relevant metals on oxide films. The deposited metal particles can easily rearrange and sinter during the course of thermally activated catalytic reactions, even at moderate temperatures.[4,5] This may lead to a decrease in their catalytic activity, which is indeed a drawback of oxide-supported metal catalysts. However, still many fundamental aspects of the growth and sintering kinetics are not fully understood.

Recent experimental studies have revealed many interesting growth behaviors of Au particles on rutile TiO_2(110).[6,7] These include (1) for low coverage (<0.1 ML) Au particle growth at room temperature shows a two-dimensional- (2-D-) like mode, and then transitions to a three-dimensional- (3-D-) like growth mode when coverage exceeds 0.1 ML; (2) at the early stages of growth, Au particles are likely to be elongated in the direction of bridging oxygen rows; (3) Au particles nucleate preferably at the sites of O vacancies; and (4) with an increase in the number of O vacancies the number of Au particles increases while the average particle size decreases.

Over recent years several research groups worldwide have attempted to address theoretically the growth and properties of Au on oxide supports, such as the adsorption and structure of small Au particles and thin Au layers on TiO_2(110)[8–11] and the reactivity of isolated small Au particles and oxide-supported thin Au strips.[12–14] However, still no clear account is available for delineating collectively the growth mode transition, elongated structures, nucleation sites, and O-vacancy assisted nucleation of Au particles on TiO_2(110).

In this paper, we present the early stage of Au particle growth on rutile TiO_2(110) based on first principles calculations. We first examine the adsorption and diffusion of a single Au atom on both stoichiometric and reduced TiO_2(110) surfaces. Then, we determine the structure and bonding of small Au_n particles ($n=1$–4) on a reduced surface, with a comparison to their gas-phase counter parts. Results from this first principles study provide valuable insight into the intriguing growth behavior of Au particles on TiO_2(110).

II. COMPUTATION TECHNIQUES

All our DFT calculations were performed within the generalized gradient approximation (PW91).[15] using plane-wave basis sets and ultrasoft pseudopotentials,[16] as implemented in the Vienna Ab-initio Simulation Package (VASP).[17] A plane-wave cutoff energy of 300 eV was used. The atomic structures, adsorption energies, and diffusion barriers of Au adatoms and particles were mostly calculated using a 15 atomic-layer (2×3) slab that is separated from its periodic images by a vacuum space of 10 Å. (Note that the three-atomic layer corresponds to one O-Ti-O layer that has also been commonly adopted in the literature.) Au atoms and all surface atoms in the top nine atomic layers were fully relaxed using the conjugate gradient method until residual forces on the flexible atoms become smaller than 5×10^{-2} eV/Å. For the Brillouin Zone integration, unless specified otherwise, we used a $(2\times4\times1)$ Monkhorst-Pack mesh of k points for a (2×3) surface cell. We considered spin polarization, but it turns out to affect insignificantly the final atomic structures and energetics. The chosen parameters have been proven to be sufficient for describing the Au-TiO_2(110) system.[11] We used the nudged elastic band method.[18] with eight intermediate images in the search of diffusion pathways and barriers.

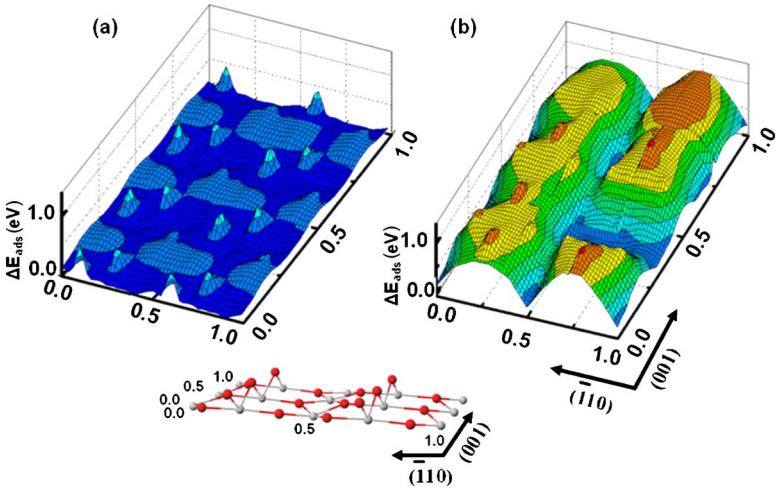

FIG. 1. (Color online) Potential energy maps for a single Au atom on (a) stoichiometric and (b) reduced TiO_2(110) surfaces. The relative adsorption energies (ΔE_{ads}) in eV are calculated with respect to the lowest adsorption energy on each (2×3) surface cell considered. On the schematic of the stoichiometric Ti(110) surface (inset), the red (dark grey) and grey balls represent O and Ti atoms, respectively.

III. RESULTS AND DISCUSSION

The stoichiometric TiO_2(110) surface (Fig. 1, inset) consists of two types of Ti atoms and two types of O atoms: five-fold coordinate Ti(5*c*), six-fold coordinate Ti(6*c*) atoms, two-fold coordinate (protruding) bridging oxygen O(2*c*), and three-fold coordinate in-plane O(3*c*) atoms. A reduced surface is prepared by removing a bridging O(2*c*) atom from a given surface cell. The Ti(6*c*) atoms initially bonded to the removed O(2*c*) atom become five-fold coordinated; [they are hereafter labeled as $Ti(6c)_d$]. The removal of a neutral bridging O(2*c*) atom results in two unpaired electrons that are greatly delocalized along the neighboring Ti(5*c*) rows.[9,10,19] This leads to a strong repulsive interaction between vacancies located adjacent to each other along the row.[10] As a result, the formation of vacancy pairs or larger vacancy clusters is energetically unfavorable, relative to isolated vacancies.[9,10] In fact, STM (Scanning Tunneling Microscope) measurements have shown that the majority of oxygen vacancies remain isolated.[20] While there is still some theoretical controversy over the electron localization to neighboring Ti sites,[9,19,21–24] a line scan STM measurement[20] (of showing a fairly uniform tunneling distance in the constant current mode over all Ti atoms, beneath the vacancy and neighboring Ti rows) suggests a possible partial reduction of neighboring Ti(5*c*) sites.[25] The partial reduction of Ti(5*c*) sites are also thought to facilitate the charge-transfer stabilization of O_2 molecules.[25]

Figure 1 shows the potential energy maps for a single Au adatom on the stoichiometric (a) and reduced (b) rutile TiO_2(110) surface. The reduced surface contains one oxygen vacancy per periodic (2×3) surface cell that corresponds to a vacancy concentration of approximately 17%. This comparison clearly demonstrates the presence of oxygen vacancies on TiO_2(110) significantly alters the adsorption and surface diffusion of single Au atoms, which will in turn affect Au particle nucleation and growth. For the potential energy maps of the stoichiometric and reduced surfaces, we sampled, respectively, (1×2) and (2×3) surface area by breaking them up into 120 and 700 evenly spaced points. We then linearly interpolated energies between neighboring points. Here, we used $(4\times4\times1)$ and $(2\times4\times1)$ Monkhorst-Pack meshes of k points for the (1×2) and (2×3) surface cells, respectively. We employed nine atomic-layer slabs to reduce a load of computation, sufficient for obtaining reasonable potential energy surfaces.[9–11] The adsorption energies and diffusion barriers reported below are, however, calculated using 15 atomic-layer slabs.

On the stoichiometric surface, the most stable Au adsorption site is the four-fold hollow position over the Ti(5*c*) and the in-plane and bridging O(2c) atoms.[9,10] In fact, the Au adsorption energy varies insignificantly, ranging from 0.4 to 0.6 eV, except for the sites atop in-plane O(3*c*) atoms, which turns out to be the most unfavorable (noted by the energy peaks). This potential energy map suggests there is no preferential diffusion direction for a single Au adatom on the stoichiometric surface.

On the reduced surface, the most energetically favorable site (noted by the potential energy valley) is the oxygen vacancy site. As summarized in Fig. 2, the vacancy site (site 0) is predicted to be approximately 1.0 eV more favorable than a bridge site between two protruding O(2*c*) atoms on the neighboring row (site 3). The bridge site is taken as a reference point because the Au adsorption energy at this site is insignificantly affected by the O vacancy. (Note that the bridge site is 0.2 eV less favorable than the most stable four-fold hollow site on the stoichiometric surface.) We also find

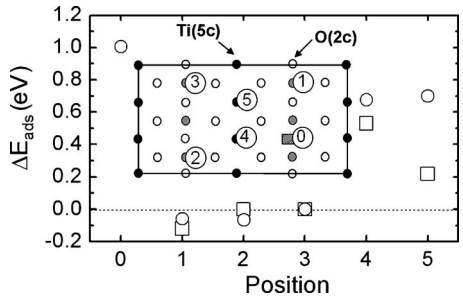

FIG. 2. Relative Au adsorption energies in eV at various positions with respect to the bridge site between two O(2*c*) atoms (site 3), with (squares) and without (circles) an Au atom at the vacancy site (site 0). The other sites considered include two O(2*c*)-O(2*c*) bridge sites, either in the same row (site1) or in the neighboring row of the vacancy (site 2); two Ti(5*c*) atop sites (sites 4 and 5).

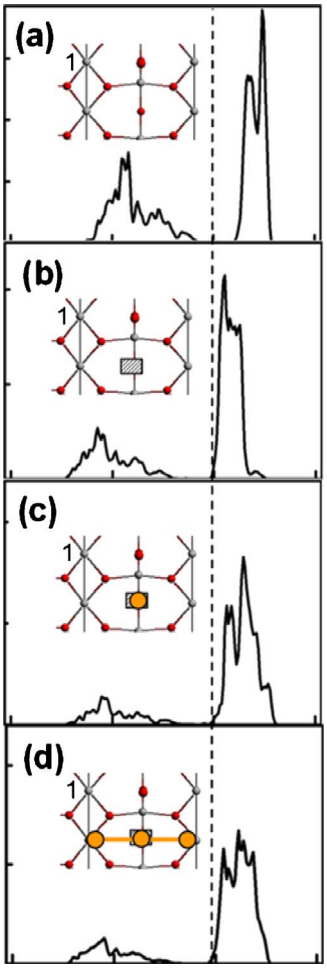

FIG. 3. (Color online) Local density of states (LDOS) of a Ti(5*c*) surface atom (as indicated 1, inset) (a) on the stoichiometric surface, (b) reduce surface, (c) with an Au atom at the vacancy site, and (d) with an Au_3 particle at the vacancy site. On the insets, the shaded square, red (dark grey) balls and grey balls represent the O vacancy, Ti(5*c*), and O(2*c*) atoms. The Au atoms are also depicted in orange (large grey). Au_2 adsorption (not shown here) exhibits a similar characteristic in the LDOS of Ti(5c) to the Au and Au_3 cases.

that there are several local energy minima [that correspond to the sites atop Ti(5*c*) atoms] on the neighboring Ti(5*c*) rows. Au adsorption energies at the sites atop Ti(5*c*) atoms (sites 4 and 5) are approximately 0.3 eV lower than at the vacancy site. The calculated barrier for Au diffusion along the Ti(5*c*) row is 0.41 eV (from site 5 to site 4 in Fig. 2). Given the sizable diffusion barrier, we suspect that Au particles could nucleate not only at O-vacancy sites but also at neighboring Ti(5*c*) sites when the Au deposition rate is sufficiently higher than the surface diffusion rate.

Next we look at how Au adsorption at the vacancy site influences subsequent Au adsorption and diffusion. When an Au atom is placed at the vacancy site, the adsorption site atop the Ti(5*c*) atom (site 5) is 0.22 eV more stable than the O(2*c*) bridge site (site 3) (as opposed to 0.70 eV with no Au at the vacancy site). The energy barrier for Au to diffuse along the Ti(5*c*) row (from site 5 to site 4 in Fig. 2) also

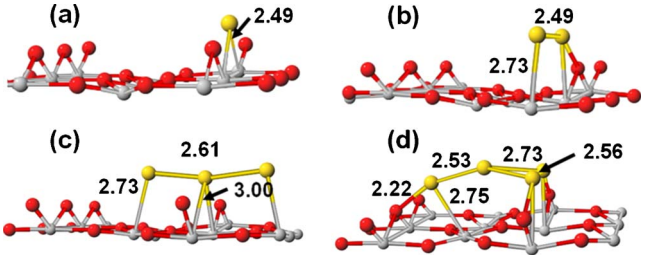

FIG. 4. (Color online) Ground state structures of the (a) Au atom, (b) dimer, (c) trimer, and (d) tetramer at the vacancy site. Yellow (large grey), red (dark grey), and grey (small grey) balls represent Au, O, and Ti atoms, respectively. The bond lengths are given in Å.

decreases to 0.26 eV. An Au atom atop one of the nearest neighboring Ti(5*c*) (site 4) can easily form a dimer with no barrier by interacting with an Au atom at the vacancy site. (When the vacancy site is occupied by an Au atom, the large Au adsorption energy difference between sites 4 and 5 is attributed to a strong interaction with the Au atom at the vacancy site.) The barrier for the dimer to swing so that it is centered across the vacancy is 0.34 eV.

Electron delocalization from O vacancies is mainly responsible for the increase in Au adsorption energy on the neighboring Ti(5*c*) rows. Figure 3 shows the projected local density of states (PDOS) of the Ti atom (as indicated) on the stoichiometric surface (a), reduced surface (b), with Au adsorbed on the vacancy site (c), and with Au_3 adsorbed on the vacancy site (d). This analysis suggests that neither of the small Au_n particles ($n \leqslant 4$) examined here fully reoxidizes the reduced surface. Recent high resolution STM measurements at temperatures lower than 300 K suggest that the number of Au atoms per vacancy is roughly constant and equal to three to five atoms. Therefore, we could expect that Ti(5*c*) rows [adjacent to O(2*c*) rows with vacancies] may provide low-energy diffusion channels for single Au adatoms, which in turn results in the growth of elongated Au particles along the [001] direction. This is consistent with CCT-STM observations that have revealed the formation of elongated shapes of Au particles in the [001] direction at the early stages of growth (<1 ML).[6]

Figure 4 shows the lowest-energy configurations of Au dimer, trimer, and tetramer anchored at the vacancy site of reduced TiO_2(110). The comparison between these supported and gas-phase particles will provide some insights into the substrate effect on the structure of small Au particles. The lowest-energy states of supported particles were identified from an extensive search, with several starting configurations. Other local minimum structures will be reported elsewhere.[26] As shown in Fig. 5, the analysis of charge density differences upon particle adsorption provides a reasonable physical picture for particle-substrate bonding mechanisms.

As discussed below, these results clearly show that the structure of small Au particles dispersed on reduced TiO_2(110) can be determined by a combination of (i) particle ionization by charge transfer from the substrate, (ii) particle-substrate bonding interaction, and (iii) geometric constraint

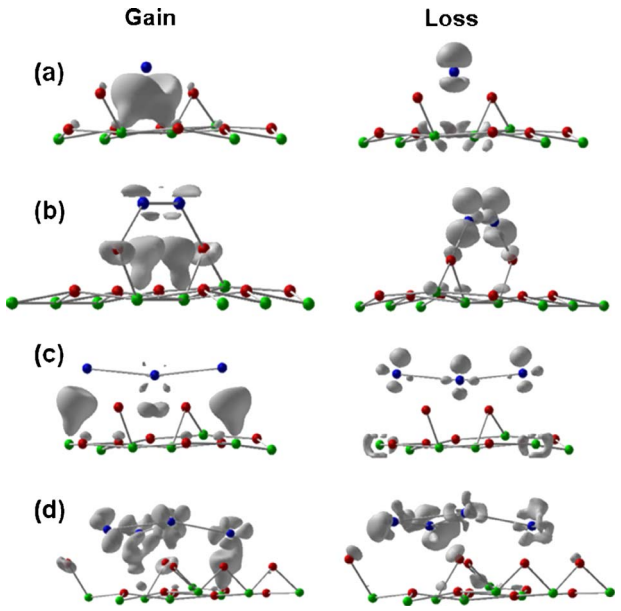

FIG. 5. (Color online) Charge density differences upon the adsorption of the (a) Au atom, (b) dimer, (c) trimer, and (d) tetramer at the vacancy site. These plots are constructed by subtracting the charge densities of isolated $Au_n(n=1–4)$ and reduced TiO_2 from those of each corresponding Au_n/TiO_2 system (as shown in Fig. 4) with no atomic displacement.

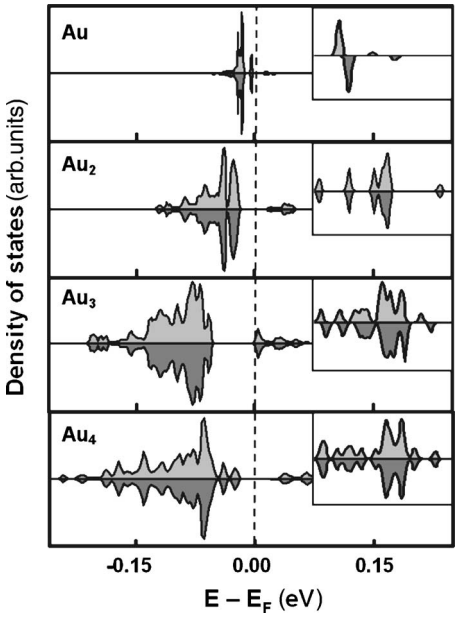

FIG. 6. Density of states for the spin up (↑) and spin down (↓) electrons of Au particles on the reduced surface. The DOS of gas-phase particles are shown in insets. The dashed vertical line at $E=0$ eV indicates the Fermi level.

by the surface structure of the support. In particular, the particle-substrate charge transfer could contribute greatly to stabilizing the adsorption of odd-numbered Au particles on the reduced surface by virtue of spin pairing.[27] Indeed we find the adsorption energy oscillates with the number of Au atoms, i.e., 1.75, 1.36, 1.91, and 1.53 eV for the Au monomer, dimer, trimer, and tetramer anchored at the vacancy site, respectively. [The adsorption energy was calculated as $E_{ad}=E(Au_n/r-TiO_2)-E(r-TiO_2)-E(Au_n)$, where $E(Au_n/r-TiO_2), E(r-TiO_2)$, and $E(Au_n)$ are, respectively, the total energies of the $Au_n/r-TiO_2$ adsorption system, the reduced TiO_2 surface, and the lowest-energy gas-phase counterpart, i.e., linear, isotriangle, and Y-shaped, respectively, for dimer, trimer, and tetramer (*vide infra*).] As shown in Fig. 6, the DOS (density of states) plots clearly demonstrate that the spins of not only the even-numbered but also the odd-numbered particles are all paired on the reduced surface, in contrast to the gas-phase ones.

Figure 4(b) shows the most favorable Au_2 structure that is aligned between two bridging O(2*c*) atoms along the [001] direction. This is in good agreement with previous DFT studies.[9] The dimer bond length is 2.49 Å, which is somewhat smaller than 2.54 Å for a neutral Au dimer in the gas phase. We attribute the bond length reduction primarily to a geometric constraint by the reduced surface. One might also suspect charge transfer to the Au dimer from the substrate, although it seems to be unlikely according to the charge density difference analysis, as discussed below. Moreover, anion Au particles generally have 2%–4% extended bond lengths relative to neutral ones. The analysis of charge density differences [Fig. 5(b)] shows charge accumulation in the regions between the Au and $Ti(6c)_d$ atoms, with some charge depletion in the Au *d*-type orbitals. This clearly indicates the existence of a sizable (covalent-type) bonding interaction between the Au dimer and the O(2*c*) vacancy.

For Au_3 [Fig. 4(c)], the lowest-energy configuration is linear, with an Au-Au bond length of 2.60 Å. The linear Au_3 structure is centered along the vacancy in the [−110] direction. As shown in Fig. 5(c), the analysis of charge density differences suggests that (i) two edge atoms interact covalently with the Ti(5*c*) atoms (adjacent to the vacancy), and (ii) compared to the dimer, the trimer-vacancy (covalent-type) bonding interaction is weaker (as evidenced by a much smaller charge accumulation in the region between them). However, the Au_3 adsorption is significantly stabilized by the spin pairing effect, along with a possible electrostatic interaction resulting from charge transfer from the O(2*c*) vacancy to the particle. We also examined the configurations of isotriangle and bent linear, but they, respectively, turn out to be 0.13 and 0.18 eV less favorable than the linear structure. Note that the linear, isotriangle, and bent-linear states are, respectively, favored for anionic, neutral, and cationic trimers in the gas phase.[27–29]

As shown in Fig. 4(d), the most stable Au tetramer has a Y-shaped structure that consists of a triangular portion, which has one side centered over the vacancy, and a linear portion that is centered over an adjacent Ti(5*c*) atom. From the charge density difference plot of the tetramer [Fig. 5(d)], we can expect that the tetramer adsorption is stabilized by the ionic interaction between the polarized edge Au atom and the negative O(2*c*) atom in the neighboring O(2*c*) row as well as the covalent interaction between the Au atoms on the triangular portion and the $Ti(6c)_d$ and neighboring Ti(5*c*) atoms. We also examined a rhombus-type configuration where two center atoms are aligned at the vacancy site along

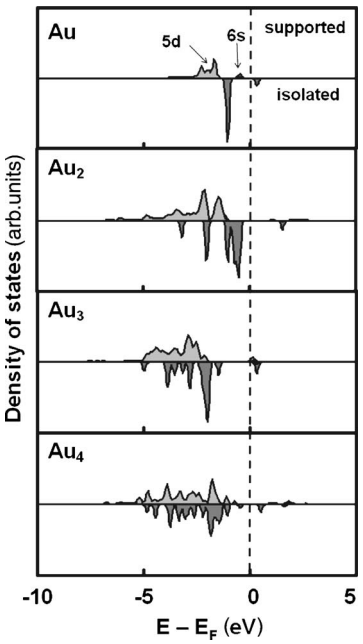

FIG. 7. A comparison of the density of states between supported and isolated (gas-phase) Au particles. The dashed vertical line at $E=0$ eV indicates the Fermi level.

the [001] direction and two edge atoms are located above adjacent Ti(5*c*) atoms, but it turns out to be 0.82 eV less stable than the Y-shaped structure. We attribute the significant difference in stability between the Y-shaped and the rhombus structures to the strong particle-substrate interaction, while possible charge transfer to the Au_4 particle from the surface could not be totally excluded. Note that, in the gas phase, neutral and anionic Au tetramers prefer rhombic and Y-shaped structures, respectively,[27,30] while the rhombic configuration is only about 0.12 eV more stable than the Y-shaped one in the neutral state. We also believe that the strong particle-substrate interaction is responsible for the two-dimensional (2D) growth of Au particles when the coverage is low.[6]

The particle-substrate interaction also results in a significant change in the electronic structure of small Au particles, as demonstrated by the comparison of PDOS between the small supported and gas-phase clusters (Fig. 7). For the Au dimer, the 6*s* state shifts far below the Fermi level as a result of the strong bonding interaction with the $Ti(6c)_d$ atoms, and also the bands are overall lower lying than in the gas phase due possibly to the hybridization with the Ti states. The energy gap between the filled 5*d* states for all the structures considered, and their gas phase counterpart decreases as you add another Au atom. The 5*d* states of the Au tetramer on the reduced $TiO_2(110)$ surface look most like the gas-phase ones, which is apparently due to the strong metallic interactions. As demonstrated here, as the particle size increases the metal-metal interaction becomes dominant over the particle-substrate interaction. This may in turn weaken the binding of particles to the substrate. As a result, 3-D growth is energetically favored for large Au particles, and their stabilization requires a number of O(2*c*) vacancies underneath (equal to 3–5 Au atoms per vacancy).[7]

IV. CONCLUSIONS

We present the growth and structure of small Au_n particles ($1 \leqslant n \leqslant 4$) on the rutile $TiO_2(110)$ surface based on plane-wave basis, pseudopotential total energy calculations. Electron delocalization from neutral O(2*c*) vacancies provides: stable Au adsorption sites atop not only vacancies but also neighboring Ti(5*c*) atoms; and low-energy Au diffusion channels along Ti(5*c*) rows. The structure of small Au particles dispersed on reduced $TiO_2(110)$ are influenced by a combination of (i) particle ionization by charge transfer from the substrate, (ii) particle-substrate bonding interaction, and (iii) geometric constraint by the surface structure of the support. The Au particle adsorption energy oscillates with the number of constituent atoms, due to the spin pairing effect for odd-numbered particles. The small Au particles at the vacancy site appear to partially reoxidize the surface, and their electronic structure is significantly altered by the particle-substrate interaction. These results offer good insight into the nucleation and early growth stages of Au deposition on $TiO_2(110)$.

ACKNOWLEDGMENTS

This work was supported by the Welch Foundation (Grant No. F-1535). GSH also thanks the NSF (CAREER-CTS-0449373 and ECS-0304026) for their partial financial support. All our calculations were performed using supercomputers in the Texas Advanced Computing Center at the University of Texas at Austin.

*Electronic address: gshwang@che.utexas.edu

[1] M. Valden, X. Lai, and D. W. Goodman, Science **281**, 1647 (1998).
[2] M. Haruta, Catal. Today **36**, 153 (1997).
[3] S. S. Lee *et al.*, J. Am. Chem. Soc. **126**, 5682 (2004).
[4] A. Kolmakov and D. W. Goodman, Catal. Lett. **70**, 93 (2000).
[5] C. T. Campbell, S. C. Parker, and D. E. Starr, Science **298**, 811 (2002).
[6] F. Cosandey and T. E. Madey, Surf. Rev. Lett. **8**, 73 (2001).
[7] E. Wahlstrom *et al.*, Phys. Rev. Lett. **90**, 026101 (2003).
[8] L. Giordano *et al.*, Surf. Sci. **471**, 21 (2001).
[9] A. Vijay, G. Mills, and H. Metiu, J. Chem. Phys. **118**, 6536 (2003).
[10] D. Pillay, Y. Wang, and G. S. Hwang, Korean J. Chem. Eng. **21**, 537 (2004).
[11] Y. Wang and G. S. Hwang, Surf. Sci. **542**, 72 (2003).
[12] Z. P. Liu, X. Q. Gong, J. Kohanoff, C. Sanchez, and P. Hu, Phys. Rev. Lett. **91**, 266102 (2003).

[13] L. M. Molina, M. D. Rasmussen, and B. Hammer, J. Chem. Phys. **120**, 7673 (2004).
[14] N. Lopez and J. K. Norskov, J. Am. Chem. Soc. **124**, 11262 (2002).
[15] J. P. Perdew *et al.*, Phys. Rev. B **46**, 6671 (1992).
[16] D. Vanderbilt, Phys. Rev. B **41**, 7892 (1990).
[17] G. Kresse and J. Hafner, Phys. Rev. B **47**, 558 (1993).
[18] G. Henkelman, B. P. Uberuaga, and H. Jonsson, J. Chem. Phys. **113**, 9901 (2000).
[19] Y. Wang, D. Pillay, and G. S. Hwang, Phys. Rev. B **70**, 193410 (2004).
[20] U. Diebold *et al.*, Surf. Sci. **411**, 137 (1998).
[21] P. J. D. Lindan, N. M. Harrison, M. J. Gillan, and J. A. White, Phys. Rev. B **55**, 15919 (1997).
[22] A. T. Paxton and L. Thien-Nga, Phys. Rev. B **57**, 1579 (1998).
[23] H. Kobayashi and M. Yamaguchi, Surf. Sci. **214**, 466 (1989).
[24] M. D. Rasmussen, L. M. Molina, and B. Hammer, J. Chem. Phys. **120**, 988 (2004).
[25] M. A. Henderson *et al.*, J. Phys. Chem. B **103**, 5328 (1999).
[26] D. Pillay and G. S. Hwang, J. Mol. Struct. (to be published).
[27] H. Hakkinen and U. Landman, Phys. Rev. B **62**, R2287 (2000).
[28] W. Andreoni and J. L. Martins, Surf. Sci. **156**, 635 (1985).
[29] X. Wu, L. Senapati, S. K. Nayak, A. Selloni, and M. Hajaligol, J. Chem. Phys. **117**, 4010 (2002).
[30] G. Mills, M. S. Gordon, and H. Metiu, Chem. Phys. Lett. **359**, 493 (2002).